Electronic Supplementary Material (ESI) for Dalton Transactions.
This journal is © The Royal Society of Chemistry 2024

Search for new biologically active compounds: *In vitro* studies of antitumor and antimicrobial activity of dirhodium(II,II) paddlewheel complexes

Marina Mitrović [a], Maja B. Djukić [b], Milena Vukić [b], Ivana Nikolić [a], Marko D. Radovanović [b], Jovan Luković [a], Ignjat P. Filipović [b], Sanja Matić [c], Tijana Marković [c], Olivera R. Klisurić [d], Suzana Popović [e], Zoran D. Matović [b], Marija S. Ristić [b,*]

[a] *University of Kragujevac, Faculty of Medical Sciences, Department of Medical Biochemistry, Svetozara Markovića 69, 34000 Kragujevac, Serbia*

[b] *University of Kragujevac, Faculty of Science, Department of Chemistry, Radoja Domanovića 12, 34000 Kragujevac, Serbia*

[c] *University of Kragujevac, Faculty of Medical Sciences, Department of Pharmacy, Svetozara Markovića 69, 34000 Kragujevac, Serbia*

[d] *University of Novi Sad, Faculty of Sciences, Department of Physics, Trg Dositeja Obradovića 4, 21000 Novi Sad, Serbia*

[e] *University of Kragujevac, Faculty of Medical Sciences, Centre for Molecular Medicine and Stem Cell Research, Svetozara Markovića 69, 34000 Kragujevac, Serbia*

*Corresponding author:
Dr. Marija Ristić, e-mail: marija.jeremic@pmf.kg.ac.rs

TABLE OF CONTENTS	page
HSA binding studies	S4
DNA-binding studies	S4
Fig. S1. ^{1}H NMR spectra of complexes **Rh1-Rh4**	S6
Fig. S2 ^{13}C NMR spectra of complexes **Rh1-Rh4**	S8
Fig. S3 IR spectra of complexes **Rh1-Rh4**	S9
Fig. S4 UV-Vis spectra of **Rh1-Rh4** complexes	S10
Fig. S5 MERCURY drawing of the overlay of the two crystallographically independent molecules of the **Rh4** complex: the molecule containing the Rh1 atom is shown in magenta, and the molecule containing the Rh2 atom in yellow	S10
Fig. S6 MERCURY drawing of the crystal packing of **Rh4** viewed along the c axis, showing C—H···O contacts (dashed line) which connect molecules in a head-to-tail manner along the *a* axis	S11
Fig. S7 Emission spectra of HSA in the presence of complexes **Rh1-Rh4**. [HSA] = 2 μM, [complex] = 0-20 μM; λex = 295 nm. The arrow shows the changes of the intensity upon increasing the concentration of complexes. The inset shows the plot of F_0/F vs. [Q]	S11
Fig. S8 HSA-ibuprofen emission spectra in the presence of **Rh1-Rh4**. [HSA] = [ibuprofen] = 2 μM, [complex] = 0-20 μM; λex = 295 nm. The arrow shows the changes of the intensity upon increasing the concentration of complexes. The inset shows the plot of F_0/F vs. [Q].	S12
Fig. S9 HSA-methyl orange emission spectra in the presence of **Rh1-Rh4**. [HSA] = [methyl orange] = 2 μM, [complex] = 0-20 μM; λex = 295 nm. The arrow shows the changes of the intensity upon increasing the concentration of complexes. The inset shows the plot of F_0/F vs. [Q].	S12
Fig S10 Emission spectra of DNA-EB (left)/DNA-HOE (right) in the absence and presence of **Rh1**. [DNA] = 100 μM; [EB/HOE] = 10 μM; [**Rh1**] = 0-180 μM for EB; 0-400 μM for HOE. λ_{ex}(EB) = 520 nm; λ_{ex}(HOE) = 346 nm. Arrow shows the changes of the intensity upon increasing the concentration of complex. The inset shows the plot of F_0/F vs. [Q]. X represents free complex.	S13
Fig S11 Emission spectra of DNA-EB (left)/DNA-HOE (right) in the absence and presence of **Rh2**. [DNA] = 100 μM; [EB/HOE] = 10 μM; [**Rh2**] = 0-180 μM for EB; 0-400 μM for HOE. λ_{ex}(EB) = 520 nm; λ_{ex}(HOE) = 346 nm. Arrow shows the changes of the intensity upon increasing the concentration of complex. The inset shows the plot of F_0/F vs. [Q]. X represents free complex.	S13
Fig S12 Emission spectra of DNA-EB (left)/DNA-HOE (right) in the absence and presence of **Rh3**. [DNA] = 100 μM; [EB/HOE] = 10 μM; [**Rh3**] = 0-180 μM for EB; 0-400 μM for HOE. λ_{ex}(EB) = 520 nm; λ_{ex}(HOE) = 346 nm. Arrow shows the changes of the intensity upon increasing the concentration of complex. The inset shows the plot of F_0/F vs. [Q]. X represents free complex.	S13
Fig. S13 Absorption spectra of **Rh1-Rh4** complexes in the absence and presence of increasing amounts of CT DNA: [complex] = 100 μM, [DNA] = 0-500 μM. Inset:	S14

linear plot for the calculation of the intrinsic DNA binding constant (K_b).	
Fig. S14 Relative viscosity $(\eta/\eta_0)^{1/3}$ of CT DNA (100 μM) in PBS buffer in the presence of the increasing amounts of complexes **Rh1-Rh4** (r)	S14
Fig. S15 Interactions of **Rh1**-**Rh4** with residues in binding site of IB domain, obtained by molecular docking.	S15
Fig. S16 Structures with the lowest energy of binding of **Rh1**-**Rh3** in the minor groove of DNA.	S15
Fig. S17 Rh1-**Rh4** inhibited the proliferation of Hela cervical, HCT116 colon, and MDA-MB-231 breast cancer cells. Cells were treated with **Rh1**-**Rh4** and cisplatin at the indicated concentrations (0.3, 1, 3, 10, 30, 60, and 100 mM) for 48h (A) and 24, 48 and 72 h (B). (A) Bar graphs show % of cytotoxic cells of triplicate readings from a representative experiment; bars, ± standard error. (B) The dose and time response curves were obtained by plotting the % of cytotoxic cells versus the log concentration of **Rh1**-**Rh4** and cisplatin used. Points, mean % of cell cytotoxicity based on quintuplicate assays, bars, ± SE. *P<0.05, **P<0.01, and ***P<0.001 vs. the control group (ctrl).	S16
Fig. S18 Effect of **Rh1**-**Rh4** on the morphology of HeLa, HCT116 and MRC-5 cells.	S17
Table S1 Selected geometric parameters for complex **Rh4**	S17
Table S2 C—H···O interactions parameters for complex **Rh4**	S18
Table S3 HSA constants (K_{sv}, k_q, K_b) and number of binding sites (n) for the interactions of **Rh1**-**Rh4** in the absence and the presence of site markers	S18
Table S4 The DNA Stern–Volmer constants (K_{sv}) and binding constants (K_b) for complexes **Rh1**-**Rh4** from CT DNA-EB and CT DNA-HOE fluorescence.	S18
Table S5 Estimated **e**nergies of binding (ΔE_b) of tested compounds with various targets, obtained from molecular docking experiments.	S19
Table S6 Selectivity index (SI) for **Rh1**-**Rh4** and cisplatin for particular tumor cells for 48h.	S19
Table S7 Crystallographic data and refinement parameters for complex **Rh4**.	S19

HSA binding studies

Fluorescence quenching is described by the Stern–Volmer equation [1]:

$F_0/F = 1 + k_q \tau_0 [Q] = 1 + K_{sv}[Q]$ (S1)

where F_0 is the emission intensity in the absence of the compound, F is the emission intensity in the presence of the compound, K_{SV} is the Stern–Volmer quenching constant, k_q is the bimolecular quenching constant, τ_0 (10^{-8} s) [2] is the lifetime of the fluorophore in the absence of the quencher, and [Q] is the concentration of the quencher (complex). The K_{SV} value is determined as the slope from the plot of F_0/F versus [Q] (**Figs. S7-S9**).

The binding constant (K) and binding stoichiometry (n) of the HSA-complex system can be estimated from the Scatchard equation [1] using the fluorescence intensity data:

$\log (F_0 - F/F) = \log K_b + n \log [Q]$ (S2)

The values of Kb and n were determined from the intercept and slope of the plots of log $(F_0 - F)/F$ *vs*. log [Q].

DNA-binding studies

Fluorescence spectroscopy

The relative binding of the complexes to the CT DNA is described by the Stern-Volmer equation [1], in the same way as described for the HSA binding studies:

$F_0/F = 1 + K_{sv}[Q]$ (S1)

where F_0 and F are the emission intensities in the absence and in presence of the quencher (complexes **Rh1-Rh4**), respectively, [Q] is the total concentration of the quencher and K_{sv} is the Stern-Volmer quenching constant, which can be determined from the slope of the plot of F_0/F *vs.* [Q] (**Figs. S10-S12**).

Absorption spectroscopy

In order to quantitatively compare the binding strength of the complexes, the intrinsic binding constants K_b were determined by observing the changes in absorbance at the MLCT band with increasing concentration of CT DNA using the Wolfe–Shimmer equation [3]:

$[DNA]/(\varepsilon_A - \varepsilon_f) = [DNA]/(\varepsilon_b - \varepsilon_f) + 1/[K_b(\varepsilon_b - \varepsilon_f)]$ (S3)

K_b is given by the ratio of the slope to the y-intercept in the plots $[DNA]/(\varepsilon_A - \varepsilon_f)$ *vs.* [DNA] (**Fig. S13**), where [DNA] is the DNA concentration in base pairs and ε_A, ε_f and ε_b are the apparent, free and fully bound complex absorption coefficients, respectively. The apparent extinction coefficient, ε_A, is determined by calculating A_{obsd}/[complex]. ε_f and ε_f correspond to

the extinction coefficient of the bound form of the complex and the extinction coefficient of the free complex.

References

[1] J. R. Lakowicz, Principles of Fluorescence Spectroscopy, Springer, New York, USA, 3rd edn, 2006.

[2] J. R. Lakowicz and G. Weber, Biochemistry, 1973, 12, 4161.

[3] A. Wolf, G. H. Shimer, T. Meehan, Biochemistry, 26 (1987) 6392–6396.

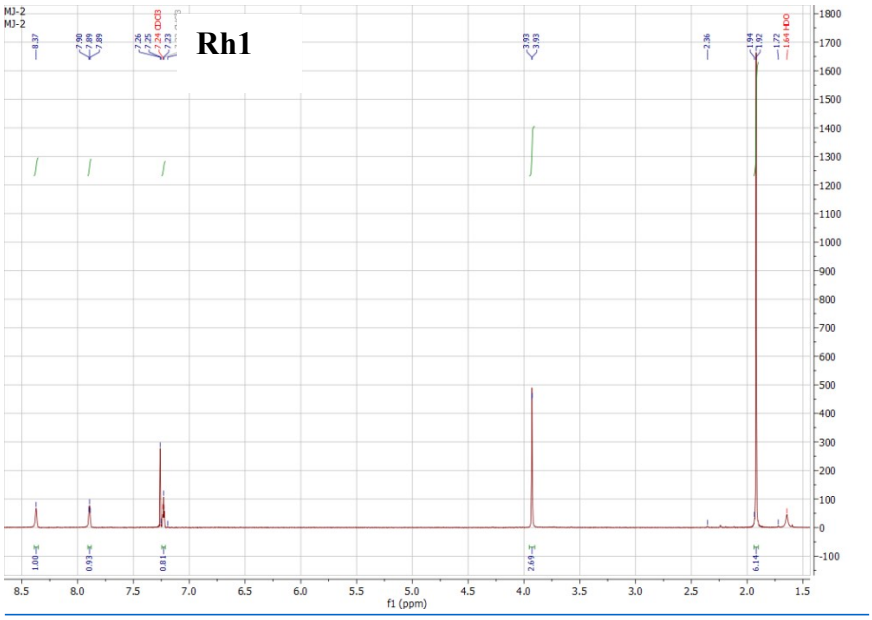

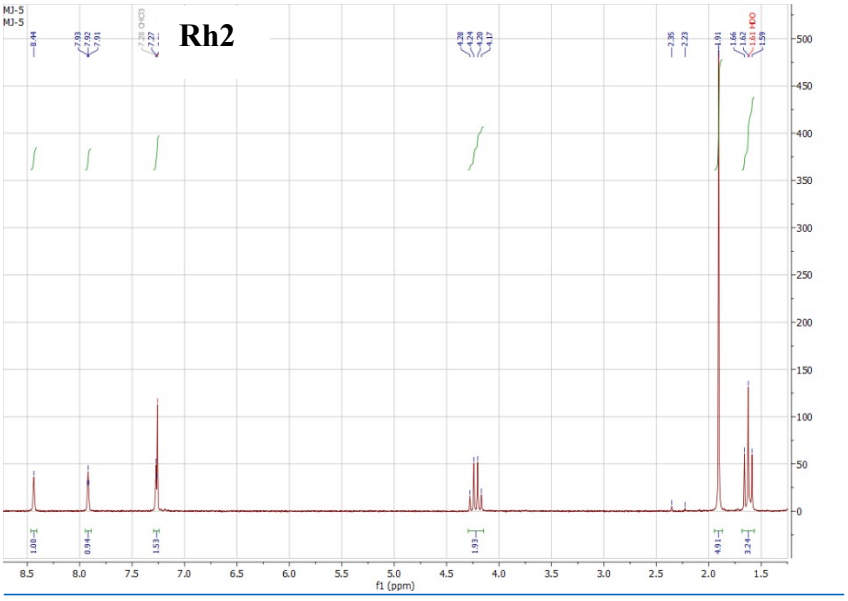

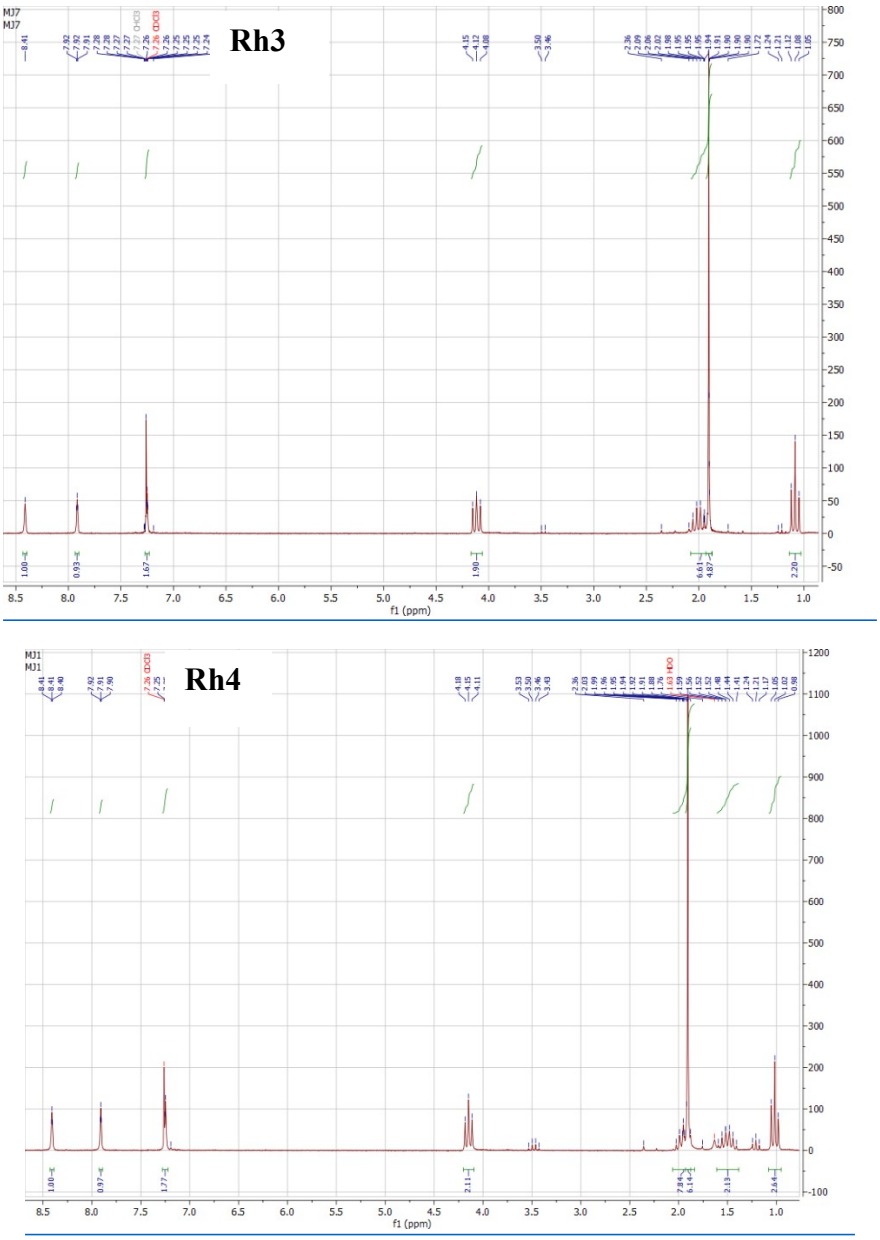

Fig. S1. ^{1}H NMR spectra of complexes **Rh1-Rh4**.

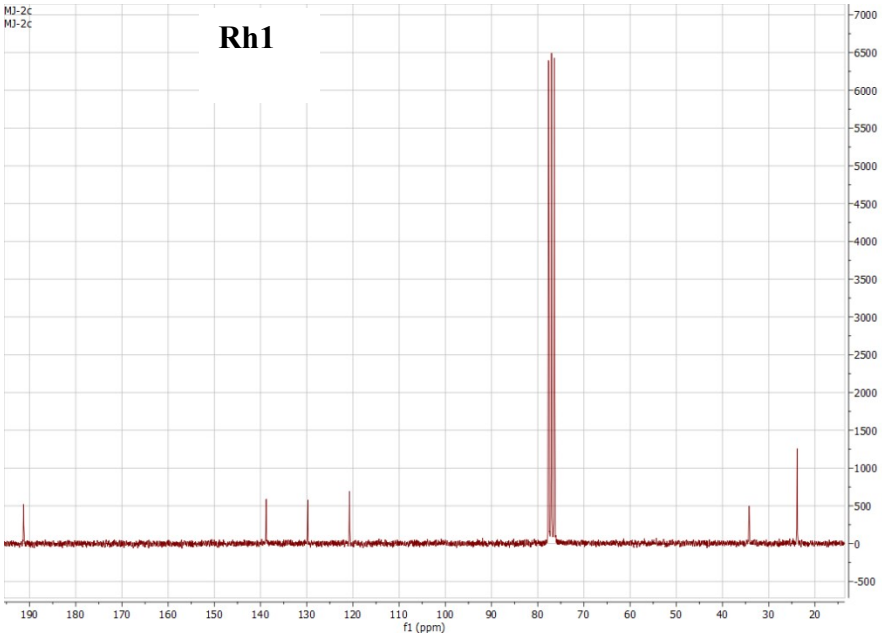
MJ-2c
MJ-2c
Rh1
f1 (ppm)

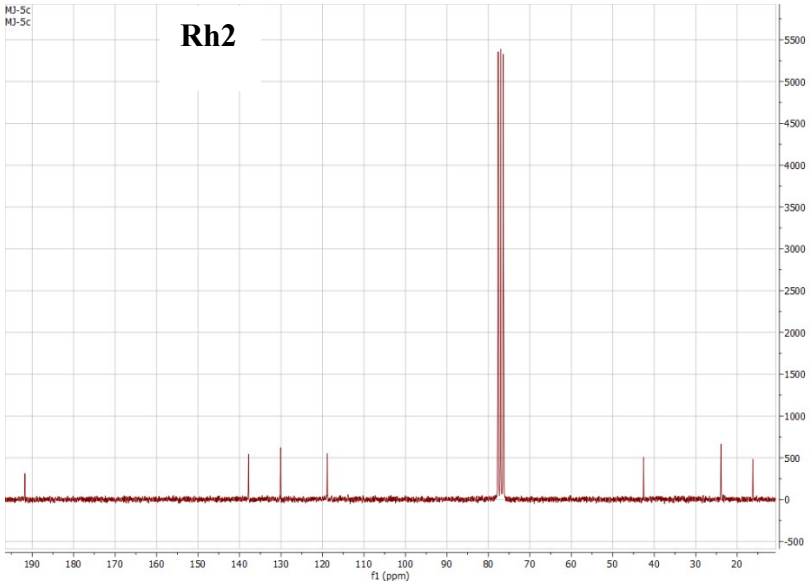
MJ-5c
MJ-5c
Rh2
f1 (ppm)

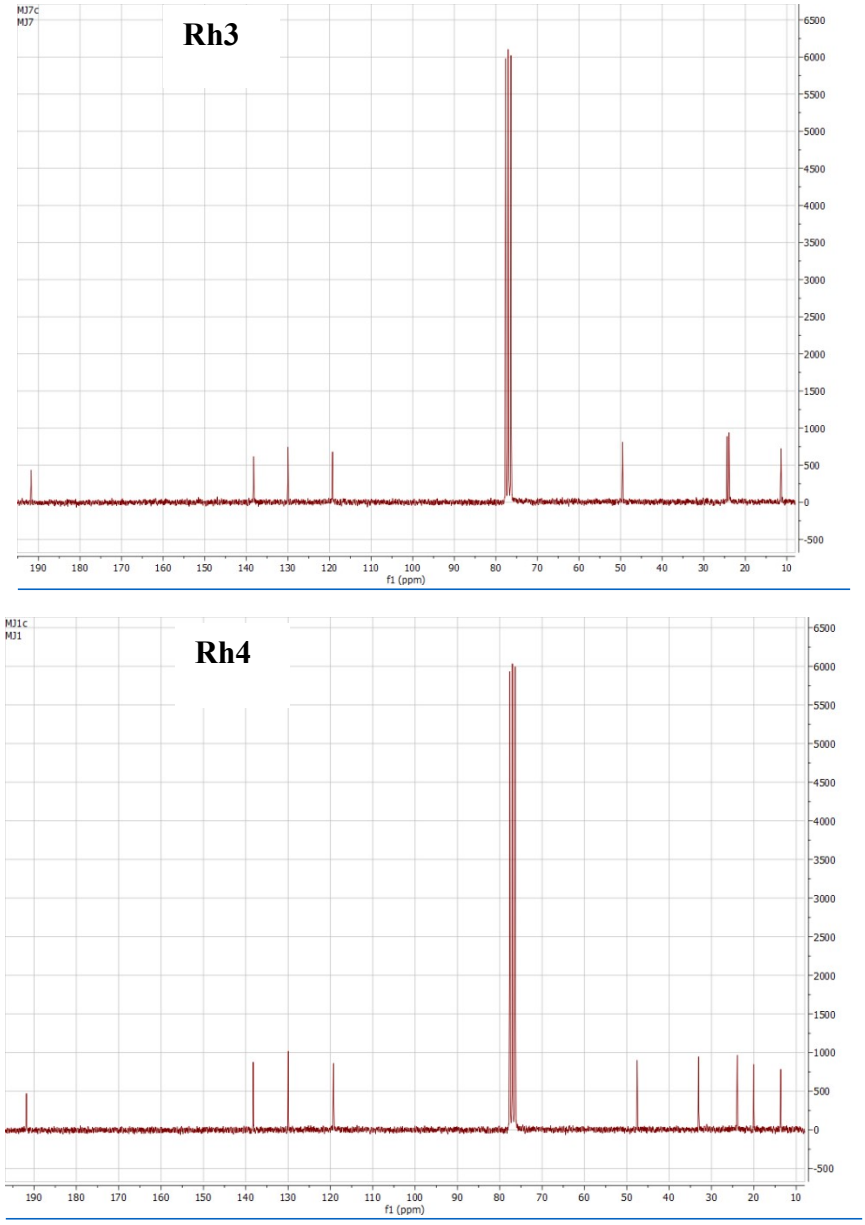

Fig. S2. ^{13}C NMR spectra of complexes **Rh1-Rh4**.

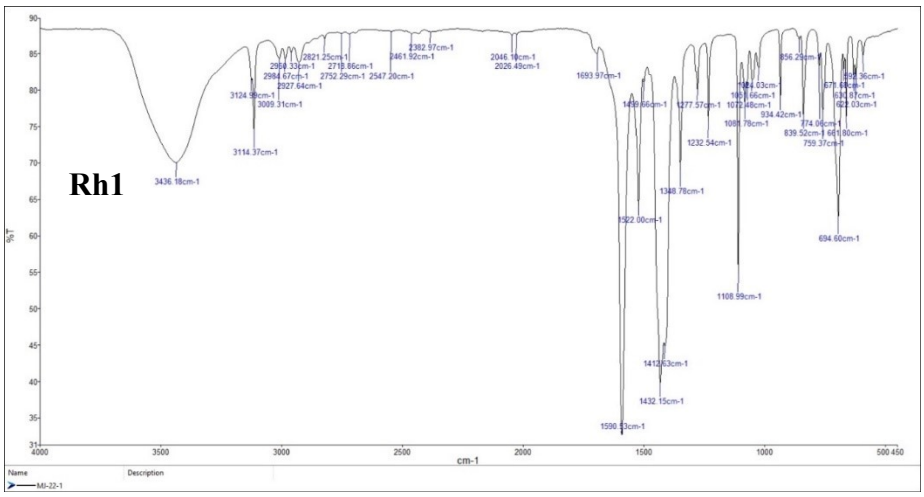

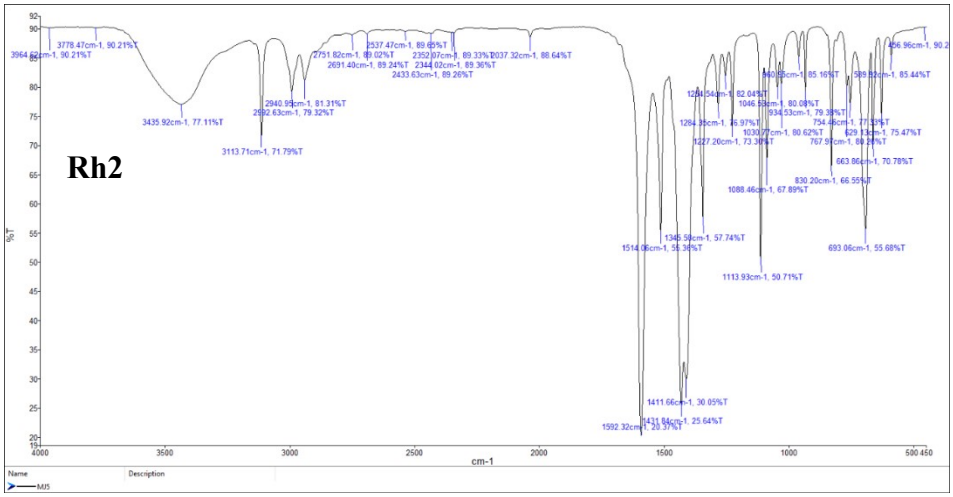

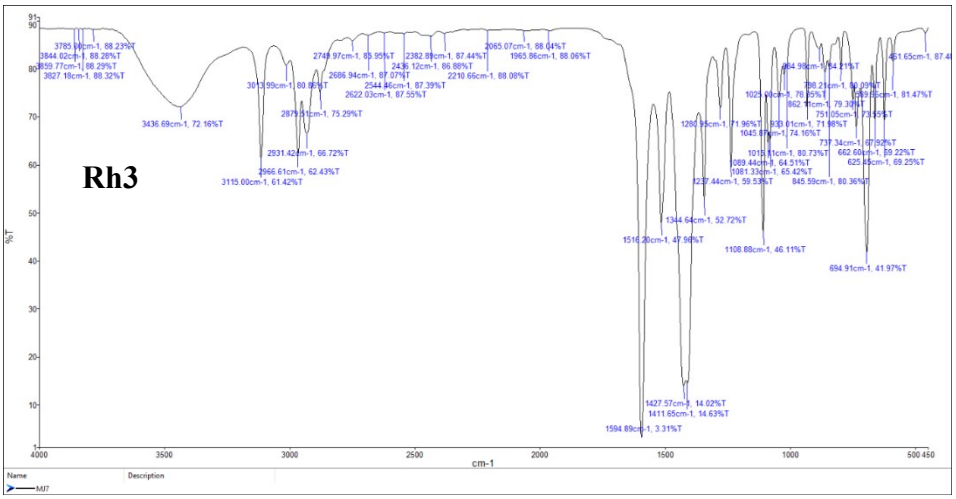

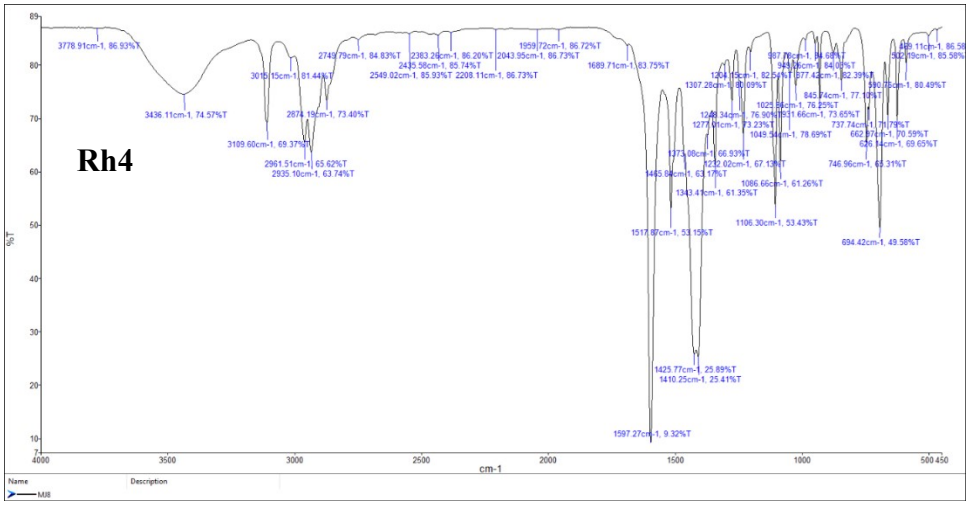

Fig. S3. IR spectra of complexes **Rh1-Rh4**.

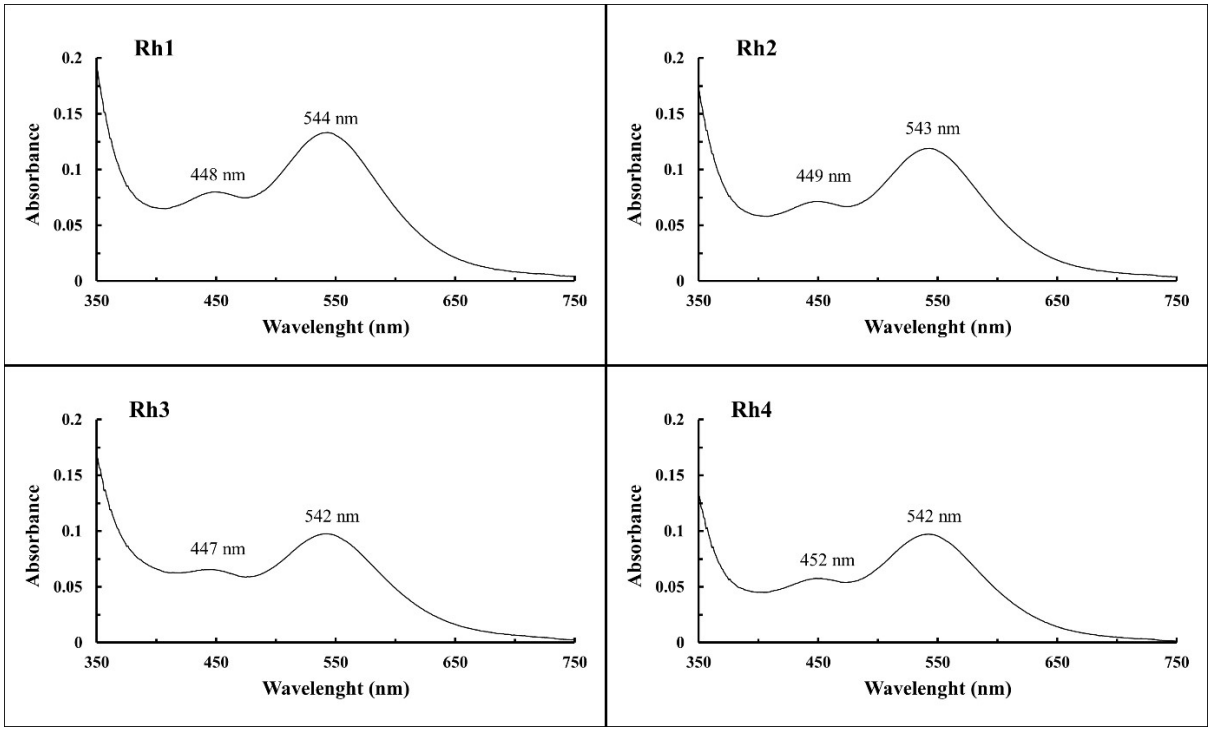

Fig. S4. UV-Vis spectra of **Rh1-Rh4** complexes

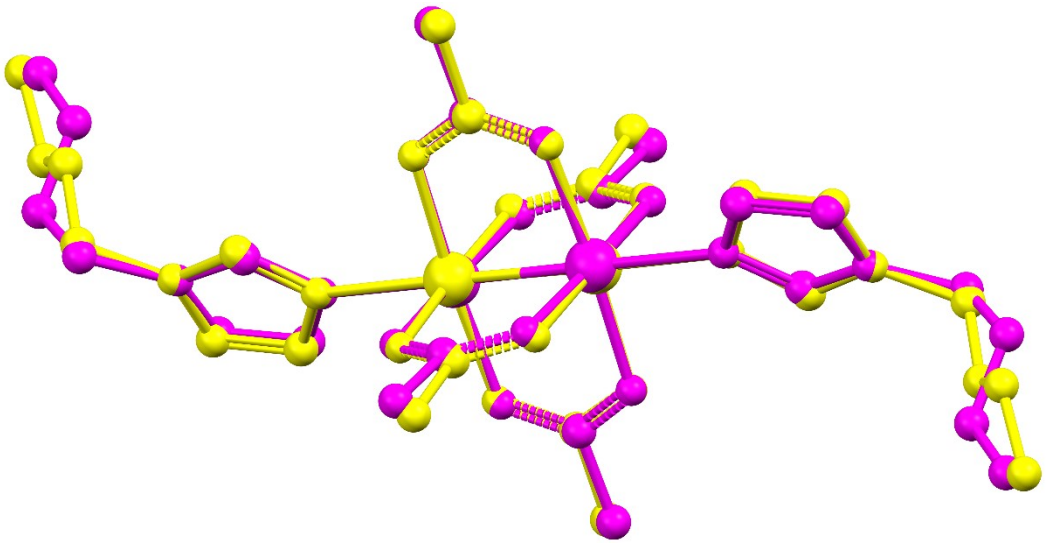

Fig. S5. MERCURY drawing of the overlay of the two crystallographically independent molecules of the **Rh4** complex: the molecule containing the Rh1 atom is shown in magenta, and the molecule containing the Rh2 atom in yellow.

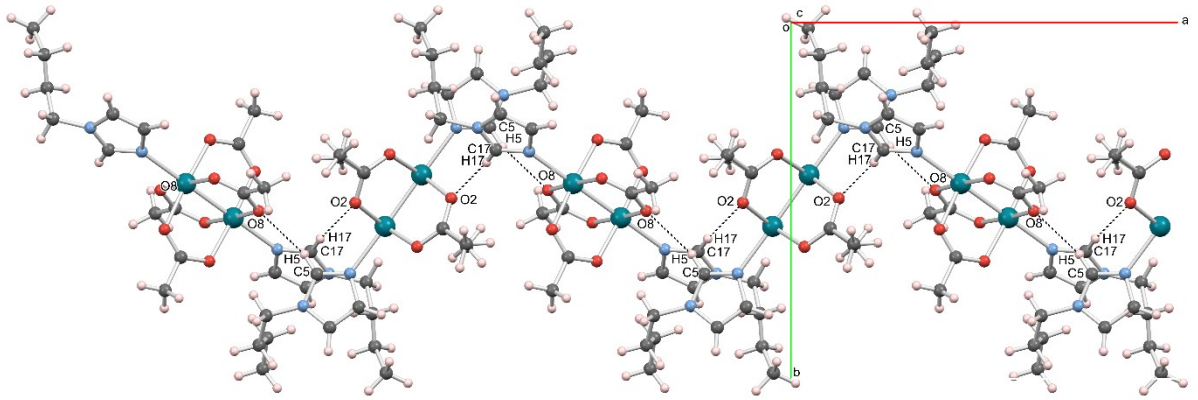

Fig. S6. MERCURY drawing of the crystal packing of **Rh4** viewed along the *c* axis, showing C—H···O contacts (dashed line) which connect molecules in a head-to-tail manner along the *a* axis.

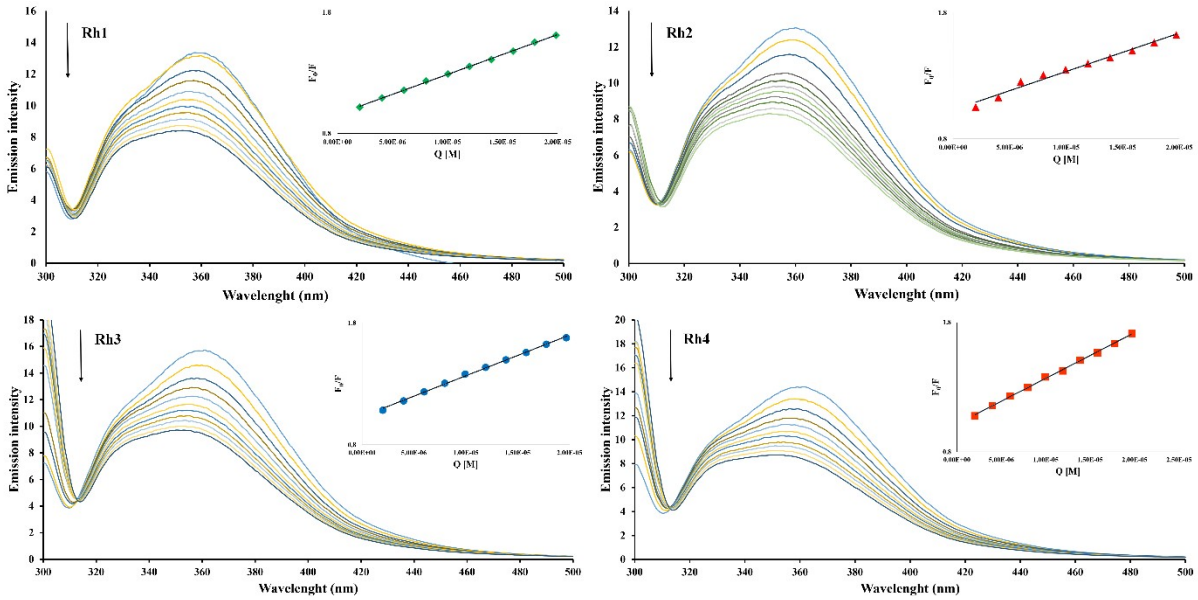

Fig. S7. Emission spectra of HSA in the presence of complexes **Rh1-Rh4**. [HSA] = 2 μM, [complex] = 0-20 μM; λ_{ex} = 295 nm. The arrow shows the changes of the intensity upon increasing the concentration of complexes. The inset shows the plot of F_0/F vs. [Q].

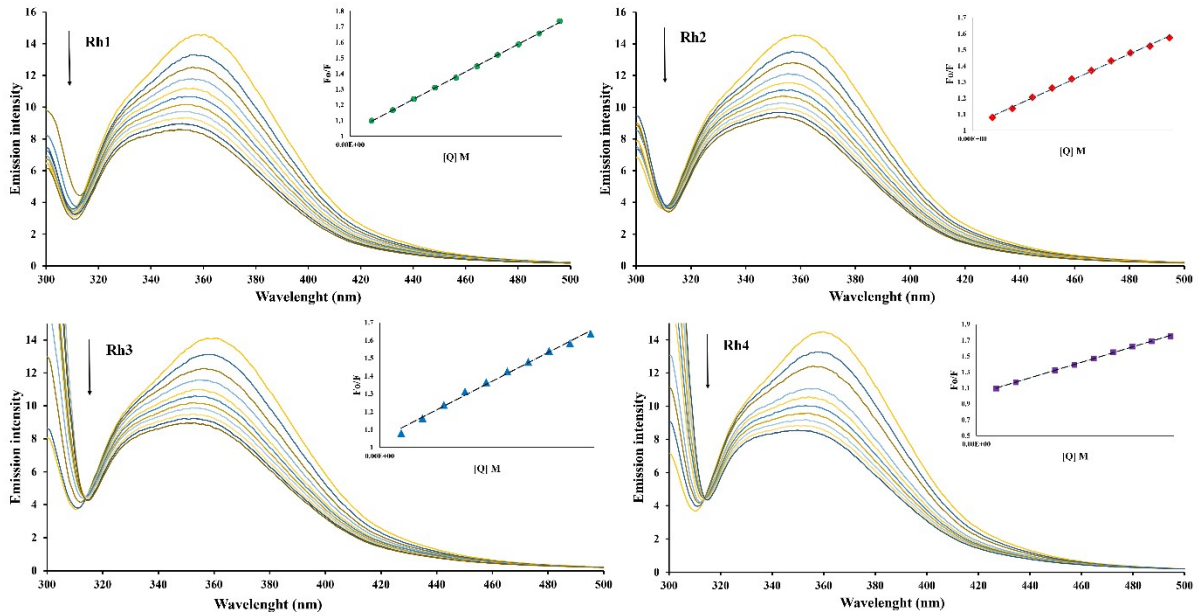

Fig. S8. HSA-ibuprofen emission spectra in the presence of **Rh1**-**Rh4**. [HSA] = [ibuprofen] = 2 μM, [complex] = 0-20 μM; λ_{ex} = 295 nm. The arrow shows the changes of the intensity upon increasing the concentration of complexes. The inset shows the plot of F_0/F vs. [Q].

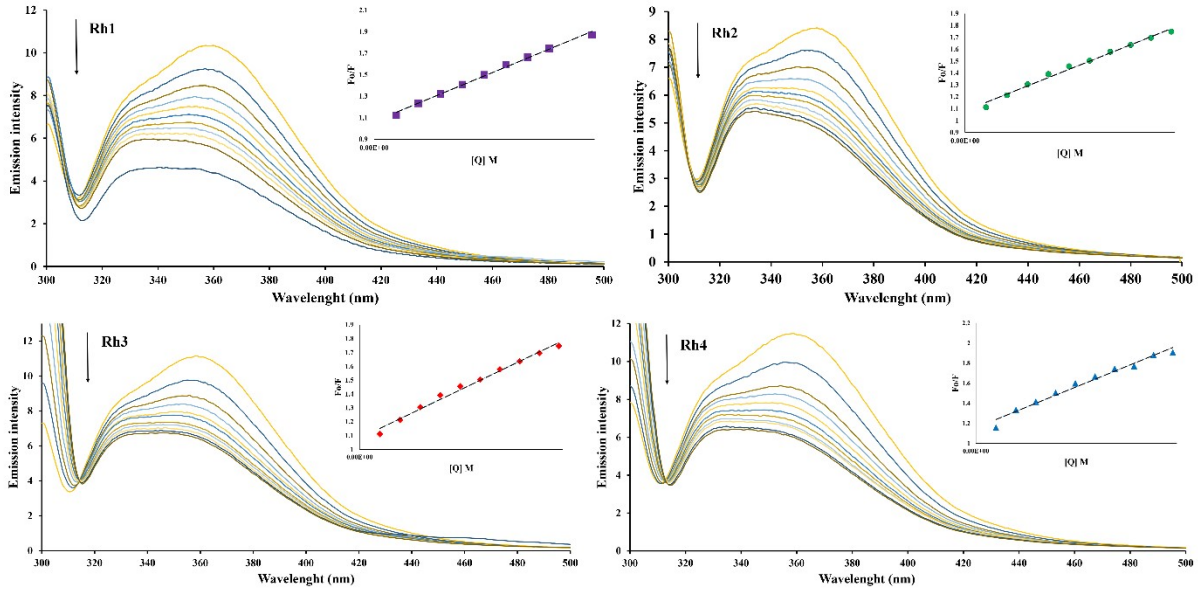

Fig. S9. HSA-methyl orange emission spectra in the presence of **Rh1** - **Rh4**. [HSA] = [methyl orange] = 2 μM, [complex] = 0-20 μM; λ_{ex} = 295 nm. The arrow shows the changes of the intensity upon increasing the concentration of complexes. The inset shows the plot of F_0/F vs. [Q].

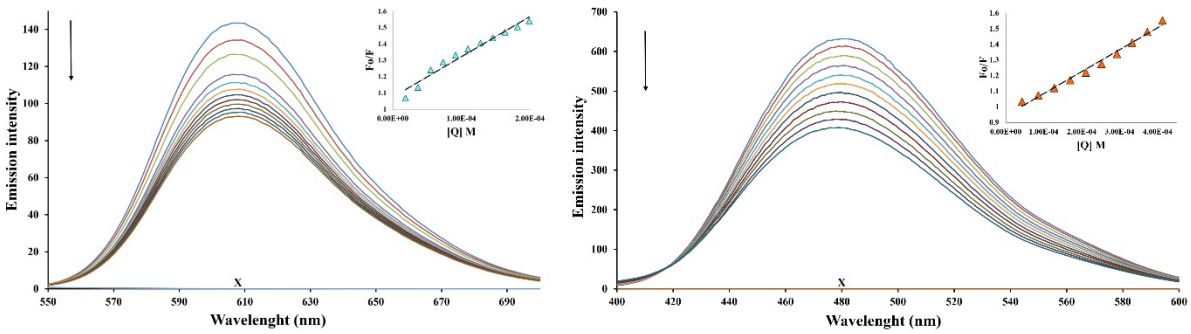

Fig S10. Emission spectra of DNA-EB (left)/DNA-HOE (right) in the absence and presence of **Rh1**. [DNA] = 100 μM; [EB/HOE] = 10 μM; [**Rh1**] = 0-180 μM for EB; 0-400 μM for HOE. $\lambda_{ex(EB)}$ = 520 nm; $\lambda_{ex(HOE)}$ = 346 nm. Arrow shows the changes of the intensity upon increasing the concentration of complex. The inset shows the plot of F_0/F vs. [Q]. X represents free complex.

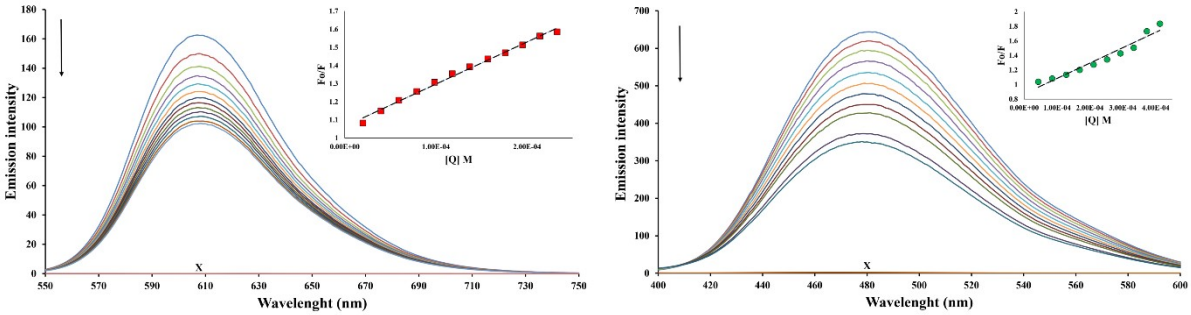

Fig S11. Emission spectra of DNA-EB (left)/DNA-HOE (right) in the absence and presence of **Rh2**. [DNA] = 100 μM; [EB/HOE] = 10 μM; [**Rh2**] = 0-180 μM for EB; 0-400 μM for HOE. $\lambda_{ex(EB)}$ = 520 nm; $\lambda_{ex(HOE)}$ = 346 nm. Arrow shows the changes of the intensity upon increasing the concentration of complex. The inset shows the plot of F_0/F vs. [Q]. X represents free complex.

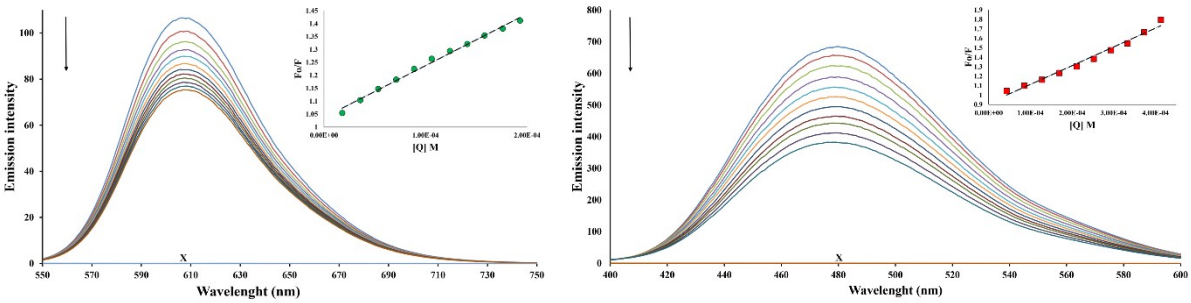

Fig S12. Emission spectra of DNA-EB (left)/DNA-HOE (right) in the absence and presence of **Rh3**. [DNA] = 100 μM; [EB/HOE] = 10 μM; [**Rh3**] = 0-180 μM for EB; 0-400 μM for HOE. $\lambda_{ex(EB)}$ = 520 nm; $\lambda_{ex(HOE)}$ = 346 nm. Arrow shows the changes of the intensity upon increasing

the concentration of complex. The inset shows the plot of F_0/F vs. [Q]. X represents free complex.

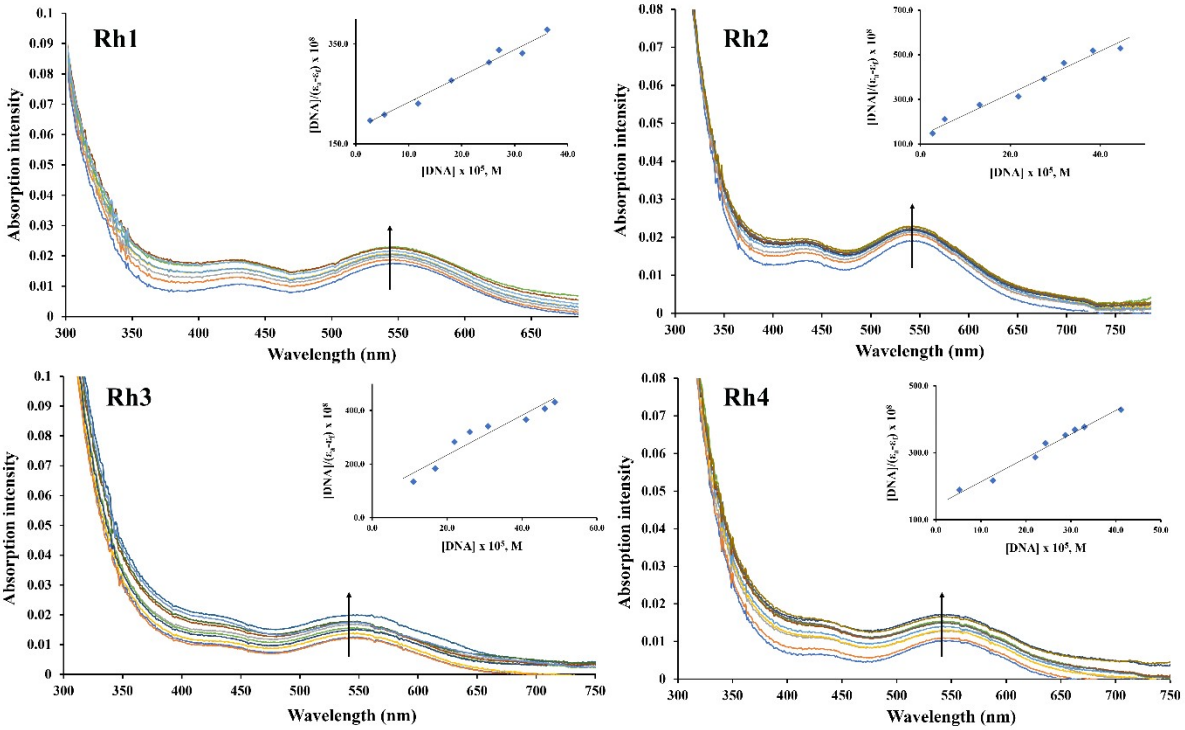

Fig. S13. Absorption spectra of **Rh1-Rh4** complexes in the absence and presence of increasing amounts of CT DNA: [complex] = 100 μM, [DNA] = 0-500 μM. Inset: linear plot for the calculation of the intrinsic DNA binding constant (K_b).

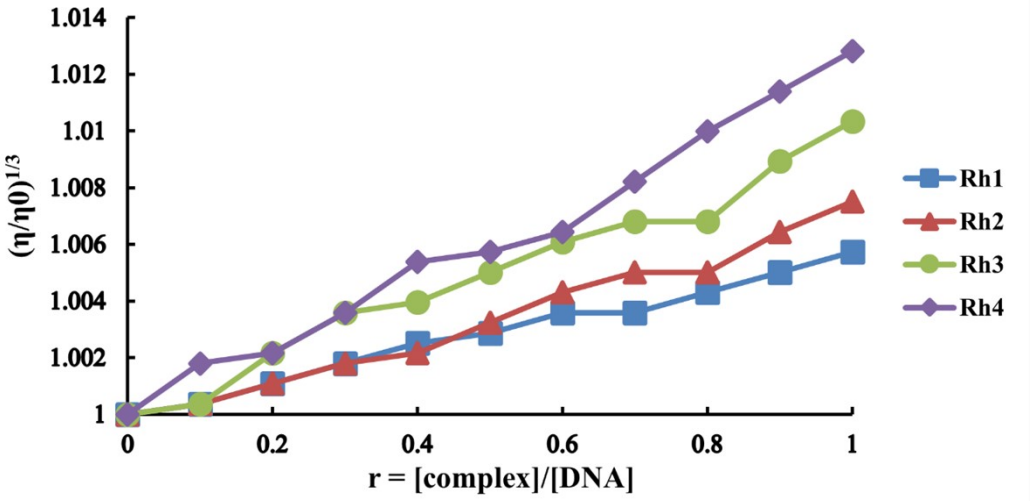

Fig. S14. Relative viscosity $(\eta/\eta_0)^{1/3}$ of CT DNA (100 μM) in PBS buffer in the presence of the increasing amounts of complexes **Rh1-Rh4** (r)

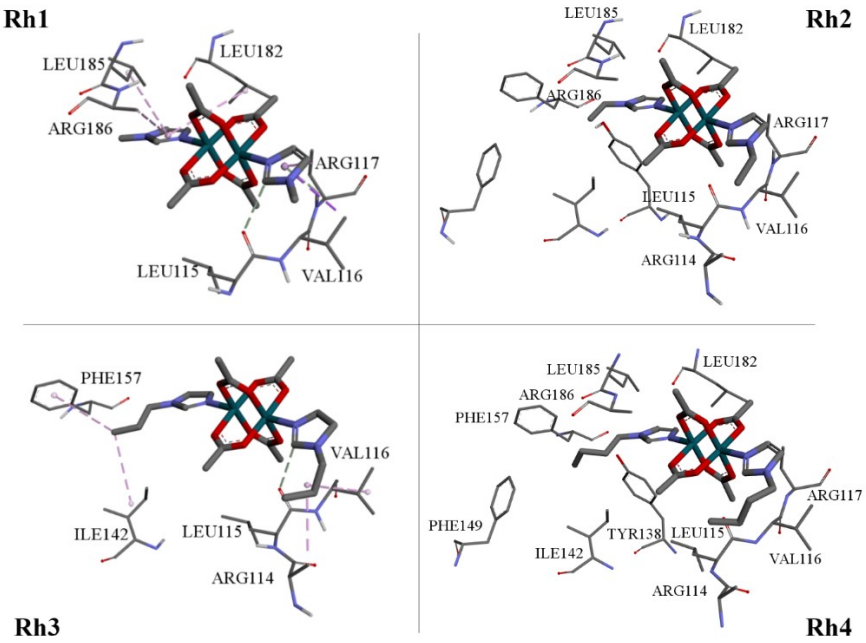

Fig. S15. Interactions of **Rh1**-**Rh4** with residues in binding site of IB domain, obtained by molecular docking.

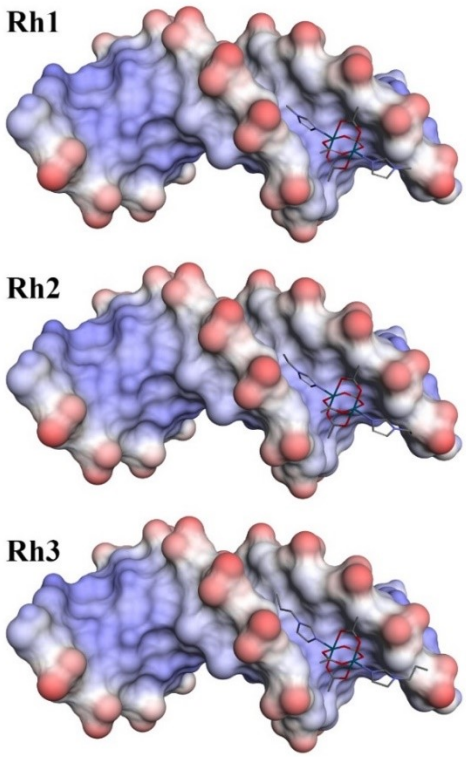

Fig. S16. Structures with the lowest energy of binding of **Rh1**-**Rh3** in the minor groove of DNA.

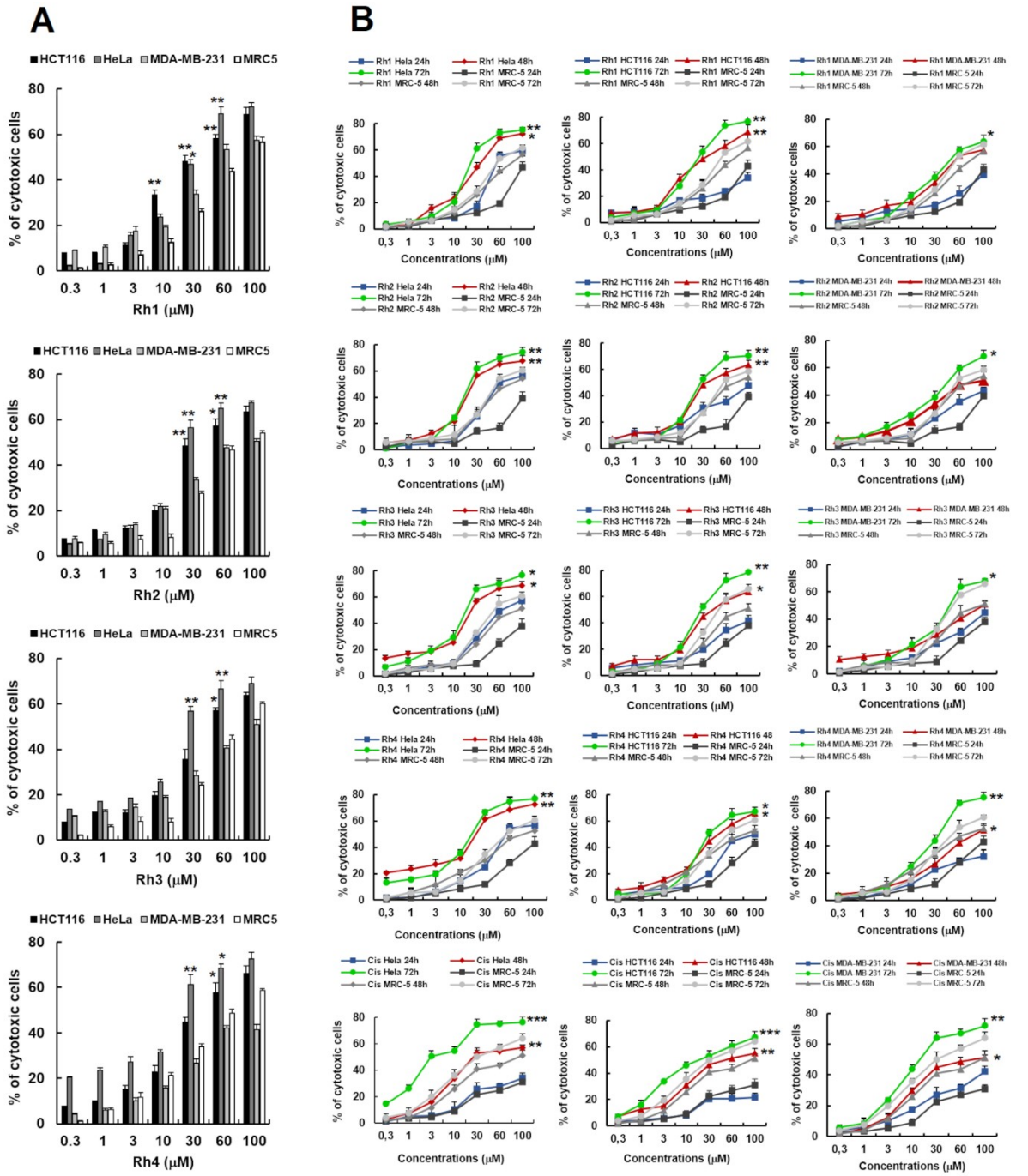

Fig. S17. Rh1-Rh4 inhibited the proliferation of Hela cervical, HCT116 colon, and MDA-MB-231 breast cancer cells. Cells were treated with **Rh1-Rh4** and cisplatin at the indicated concentrations (0.3, 1, 3, 10, 30, 60, and 100 mM) for 48h (A) and 24, 48 and 72 h (B). (A) Bar graphs show % of cytotoxic cells of triplicate readings from a representative experiment; bars, ± standard error. (B) The dose and time response curves were obtained by plotting the % of cytotoxic cells versus the log concentration of **Rh1-Rh4** and cisplatin used. Points, mean % of cell cytotoxicity based on quintuplicate assays, bars, ± SE. *P<0.05, **P<0.01, and ***P<0.001 vs. the control group (ctrl).

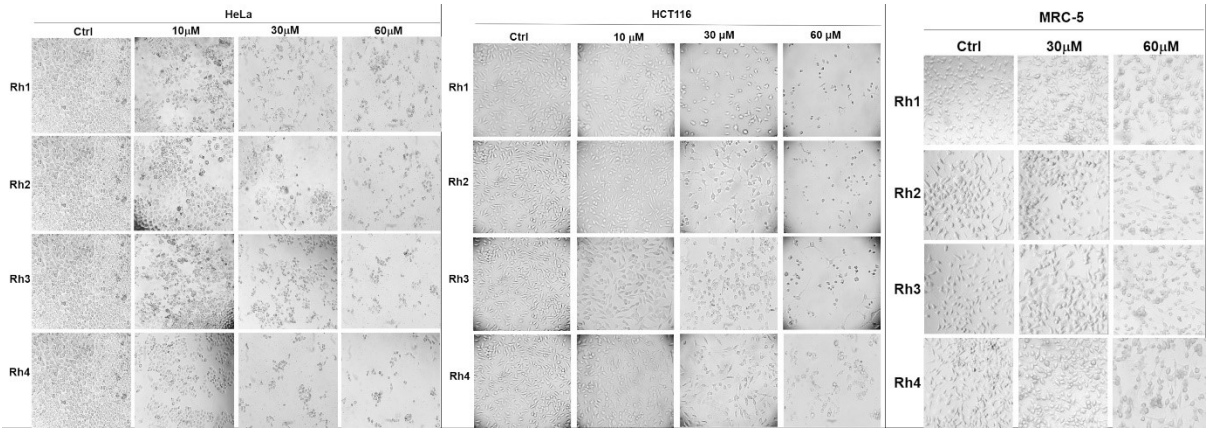

Fig. S18. Effect of **Rh1**-**Rh4** on the morphology of HeLa, HCT116 and MRC-5 cells.

Table S1 Selected geometric parameters for complex **Rh4**.

Bond length [Å]			
Rh1—O1	2.035 (4)	Rh2—O5	2.048 (5)
Rh1—O2	2.038 (4)	Rh2—O6	2.040 (4)
Rh1—O3^{i}	2.044 (4)	Rh2—O7^{ii}	2.053 (4)
Rh1—O4^{i}	2.043 (4)	Rh2—O8^{ii}	2.042 (4)
Rh1—N1	2.237 (5)	Rh2—N3	2.242 (6)
Rh1—Rh1^{i}	2.4032 (9)	Rh2—Rh2^{ii}	2.4032 (10)
Bond angles [°]			
O1—Rh1—O2	89.96 (19)	O6—Rh2—O8^{ii}	175.66 (19)
O1—Rh1—O4^{i}	90.33 (18)	O6—Rh2—O5	90.23 (19)
O2—Rh1—O4^{i}	175.85 (18)	O8^{ii}—Rh2—O5	89.16 (19)
O1—Rh1—O3^{i}	175.93 (17)	O6—Rh2—O7^{ii}	90.09 (19)
O2—Rh1—O3^{i}	89.55 (18)	O8^{ii}—Rh2—O7^{ii}	90.17 (19)
O4^{i}—Rh1—O3^{i}	89.87 (18)	O5—Rh2—O7^{ii}	175.41 (19)
O1—Rh1—N1	90.95 (18)	O6—Rh2—N3	91.53 (19)
O2—Rh1—N1	91.66 (18)	O8^{ii}—Rh2—N3	92.79 (19)
O4^{i}—Rh1—N1	92.48 (18)	O5—Rh2—N3	92.61 (19)
O3^{i}—Rh1—N1	93.10 (17)	O7^{ii}—Rh2—N3	91.96 (18)
O1—Rh1—Rh1^{i}	88.27 (13)	O6—Rh2—Rh2^{ii}	87.57 (14)
Torsion angles [°]			
Rh1—N1—C5—N2	−178.0 (4)	Rh2—N3—C17—N4	−180.0 (4)
Rh1—O2—C2—O4	0.8 (10)	Rh2—O6—C13—O8	0.8 (10)
Rh1—O2—C2—C4	−179.2 (5)	Rh2—O6—C13—C15	−179.2 (6)
Rh1^{i}—O4—C2—O2	−0.3 (9)	Rh2—O5—C12—O7	0.4 (11)
Rh1^{i}—O4—C2—C4	179.8 (5)	Rh2—O5—C12—C14	−178.3 (5)

Symmetry codes: (i) −*x*+2, −*y*+1, −*z*+1; (ii) −*x*+1, −*y*+1, −*z*+1.

Table S2 C—H···O interactions parameters for complex **Rh4**.

D—H···*A*	*D*—H (Å)	H···*A* (Å)	*D*···*A* (Å)	*D*—H···*A* (°)
C5—H5···O8^{i}	0.93	2.55	3.465 (8)	166.8
C17—H17···O2	0.93	2.45	3.364 (8)	167.4

Symmetry code: (i) −*x*+1, −*y*+1, −*z*+1.

Table S3 HSA constants (K_{sv}, k_q, K_b) and number of binding sites (n) for the interactions of **Rh1**-**Rh4** in the absence and the presence of site markers.

System	K_{SV} (M^{-1})	k_q (M^{-1} s^{-1})	K_b (M^{-1})	n
Rh1-HSA	3.30×10^4	3.30×10^{12}	1.81×10^5	1.16
Rh1-HSA-warfarin	4.05×10^4	4.05×10^{12}	7.26×10^4	1.05
Rh1-HSA-ibuprofen	3.55×10^4	3.55×10^{12}	9.90×10^3	0.88
Rh1-HSA-methyl orange	4.24×10^4	4.24×10^{12}	9.78×10^3	0.86
Rh2-HSA	3.04×10^4	3.04×10^{12}	4.47×10^4	1.02
Rh2-HSA-warfarin	2.56×10^4	2.56×10^{12}	1.33×10^4	0.94
Rh2-HSA-ibuprofen	2.81×10^4	2.81×10^{12}	7.57×10^3	0.87
Rh2-HSA-methyl orange	3.51×10^4	3.51×10^{12}	5.58×10^3	0.82
Rh3-HSA	3.34×10^4	3.34×10^{12}	1.40×10^4	0.92
Rh3-HSA-warfarin	2.70×10^4	2.70×10^{12}	2.47×10^4	0.99
Rh3-HSA-ibuprofen	3.09×10^4	3.09×10^{12}	1.04×10^4	0.89
Rh3-HSA-methyl orange	3.52×10^4	3.52×10^{12}	5.62×10^3	0.82
Rh4-HSA	3.53×10^4	3.53×10^{12}	2.23×10^4	0.96
Rh4-HSA-warfarin	2.83×10^4	2.83×10^{12}	1.19×10^4	0.92
Rh4-HSA-ibuprofen	3.74×10^4	3.74×10^{12}	1.45×10^4	0.91
Rh4-HSA-methyl orange	4.09×10^4	4.09×10^{12}	2.80×10^3	0.74

Table S4 The DNA Stern–Volmer constants (K_{sv}) and binding constants (K_b) for complexes **Rh1**-**Rh4** from CT DNA-EB and CT DNA-HOE fluorescence.

Complex	$K_{SV(EB)}$ [M^{-1}]	$K_{b(EB)}$ [M^{-1}]	$K_{SV(HOE)}$ [M^{-1}]	$K_{b(HOE)}$ [M^{-1}]	K_b [a] [M^{-1}]
Rh1	2.03×10^3	7.79×10^2	1.59×10^3	1.39×10^4	1.05×10^4
Rh2	2.18×10^3	4.36×10^2	2.43×10^3	2.71×10^4	7.34×10^3
Rh3	1.93×10^3	5.64×10^2	2.16×10^3	1.85×10^4	1.09×10^4
Rh4	2.22×10^3	5.53×10^2	2.04×10^3	1.72×10^4	1.16×10^4

[a] UV-Vis data

Table S5 Estimated **e**nergies of binding (ΔE_b) of tested compounds with

various targets, obtained from molecular docking experiments.

Compound	ΔE_b [kcal mol^{-1}]			
	IIA	IIIA	IB	DNA
Rh1	-4.52	-4.77	-5.56	-4.00
Rh2	-4.76	-5.01	-5.79	-4.10
Rh3	-4.74	-5.05	-6.29	-4.30
Rh4	-5.36	-5.22	-6.58	-4.78

Table S6 Selectivity index (SI) for **Rh1**-**Rh4** and cisplatin for particular tumor cells for 48h.

Complex	Selectivity index (SI)								
	24h			48h			72h		
	Hela	HCT116	MDA-MB-231	Hela	HCT116	MDA-MB-231	Hela	HCT116	MDA-MB-231
Rh1	2.98	0.67	1.45	2.46	2.61	1.28	2.5	2.2	1.12
Rh2	2.03	0.65	0.82	3.13	2.21	1.01	2.7	1.96	1.16
Rh3	2.13	0.43	1.01	3.71	2.22	0.91	2.82	1.9	1.27
Rh4	1.85	0.73	<0.6	4.38	2.1	0.94	3.56	1.98	1.75
Cisplatin	<0.6	<0.6	<0.6	3.7	1.73	1.55	7.33	1.84	2.54

Table S7 Crystallographic data and refinement parameters for complex **Rh4.**

Crystal data	
Chemical formula	$2(C_{11}H_{18}N_2O_4Rh)\cdot 1[C_7H_8]$
M_r	782.51
Crystal system	Monoclinic
Space group	$P2_1/c$
a (Å)	15.7537 (6)
b (Å)	13.5490 (5)
c (Å)	17.3153 (7)
β (°)	110.366 (5)
V (Å^3)	3464.9 (3)
Z	4
D_x (Mg m^{-3})	1.500
μ (mm^{-1})	1.00
Crystal size (mm)	0.40 × 0.27 × 0.25
Crystal shape	Prism
Colour	Purple
Data collection	
Absorption correction	Multi-Scan

T_{min}, T_{max}	0.944, 1.000
Reflections collected	17655
Independent reflections	8088
Observed reflections [$I > 2\sigma(I)$]	5710
R_{int}	0.031
Range of h, k, l	h = −21→20, k = −17→17, l = −23→23
θ values (°)	θ_{max} = 29.3, θ_{min} = 2.0
Refinement	
$R[F^2 > 2\sigma(F^2)]$, $wR(F^2)$	0.0629, 0.1645
R[*all data*], $wR2$	0.0898, 0.1502
Goodness-of-fit (S)	1.065
No. of reflections	8088
No. of parameters	331
No. of restraints	34
$\Delta\rho_{max}$, $\Delta\rho_{min}$ (e Å^{-3})	1.11, −0.60
CCDC no.	2340710